Chinese Chemical Letters 34 (2023) 108192

Contents lists available at ScienceDirect

Chinese Chemical Letters

journal homepage: www.elsevier.com/locate/cclet

# Copper carbonate nanoparticles as an effective biomineralized carrier to load macromolecular drugs for multimodal therapy

Liping Dong[a], Jinsong Ding[b], Lemei Zhu[a], Yujun Liu[c], Xiang Gao[c,*], Wenhu Zhou[a,b,d,*]

[a] Changsha Medical University, Academician Workstation, Changsha 410219, China
[b] Xiangya School of Pharmaceutical Sciences, Central South University, Changsha 410013, China
[c] State Key Laboratory of Toxicology and Medical Countermeasures, Institute of Pharmacology and Toxicology, Beijing 100850, China
[d] Key Laboratory of Biological Nanotechnology of National Health Commission, Changsha 410000, China

ARTICLE INFO

*Article history:*
Received 20 October 2022
Revised 1 February 2023
Accepted 3 February 2023
Available online 5 February 2023

*Keywords:*
Metal ions
Biomineralization
Drug delivery
Nanomedicine
Tumor therapy

ABSTRACT

Macromolecular drugs have attracted great interest as biotherapy to cure previously untreatable diseases. For clinical translation, biomacromolecules encounter several common druggability difficulties, such as *in vivo* instability and poor penetration to cross physiologic barriers, thus requiring sophisticated systems for drug delivery. Inspired by the natural biomineralization *via* interaction between inorganic ions and biomacromolecules, herein we rationally screened biocompatible transition metals to biomineralize with carbonate for macromolecules loading. Among the metal ions, $Cu^{2+}$ was found to be the best candidate, and its superiority over the widely studied $Ca^{2+}$ minerals was also demonstrated. Capitalized on this finding, copper carbonate nanoparticles were prepared *via* a simple mixing process to co-load glucose oxidase (GOx) and a HIF-$\alpha$ DNAzyme (DZ), achieving ultra-high loading capacity of 61%. Upon encapsulation into nanoparticles, enzymatic activity of both drugs was passivated to avoid potential side-effects during circulation, while the drugs could be rapidly released within 1 h in response to acidic pH to fully recover their activities. The nanoparticles could accumulate into tumor *via* intravenous injection, facilitate the cell membrane penetration, and release the payloads of GOx, DZ and $Cu^{2+}$ inside cells to exert a series of anti-tumor effects. GOx caused tumor starvation by catalytic glucose consumption, and the concomitantly generated $H_2O_2$ byproduct boosted the $Cu^{2+}$-mediated chemodynamic therapy (CDT). Meanwhile, the DZ silenced HIF-$\alpha$ expression to sensitize both starvation therapy and CDT. As a result, a synergistic tumor growth inhibition was achieved. This work provides a simple method to prepare biomineralized nanoparticles, and offers a general approach for macromolecular drugs delivery *via* $Cu^{2+}$-based biomineralization.


Over the past 20 years, significant progress has been made on the development of macromolecular drugs, which has revolutionized the therapy of various diseases [1]. Macromolecular drugs mainly with nucleic acids- and proteins-based structures possess unique advantages over small molecular drugs such as extremely high specificity and affinity, and sophisticated biofunctions [2], which provides new hope for the treatment of currently intractable diseases (*i.e.*, cancer, atherosclerosis, and rheumatoid arthritis) [3,4]. However, the structural complexity of this type of drugs raises several common druggable challenges. For example, the macromolecules without chemical modifications are unstable in systemic circulation and prone to biological degradation by proteolysis (for proteins) and nucleases (for nucleic acids). In addition, macromolecules cannot freely penetrate the biological barriers and cell membrane for action because of their big size. Therefore, the development of suitable drug delivery systems is highly desired for macromolecular drugs [5–8].

Currently, extensive research attention has been paid on the design of polymer- and lipid-based nanostructures for delivery of macromolecular drugs, such as cationic polymers for siRNA and lipid nanoparticles for mRNA vaccines [9]. While great success has been made, these delivery systems have several intrinsic limitations, including tedious materials synthesis, complex preparation procedure, and potential toxicity of the carriers. In addition, the complex and large size of the drugs impose difficulty for effective encapsulation, and the loading is usually achieved *via* electrostatic interaction, which however brings the risk of pre-mature leakage during *in vivo* circulation, compromising the final efficacy. Therefore, the development of simple yet robust carriers to deliver macromolecules still remains a challenge.

* Corresponding authors.
*E-mail addresses:* gaoxiang609@163.com (X. Gao), zhouwenhuyaoji@163.com (W. Zhou).

https://doi.org/10.1016/j.cclet.2023.108192
1001-8417/

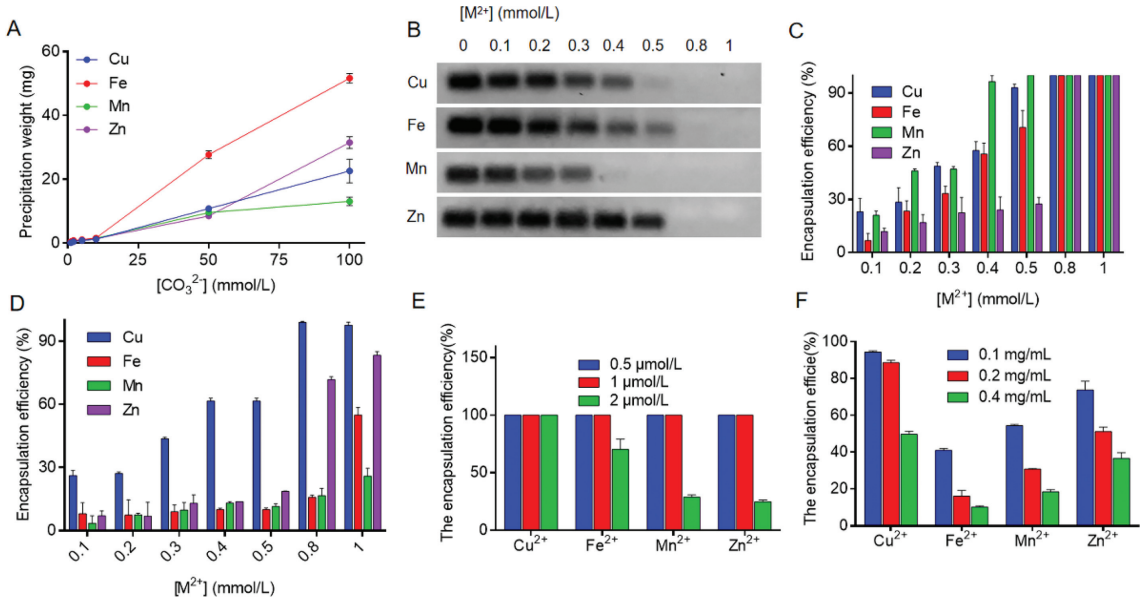


**Fig. 1.** (A) The quantification of the precipitant weights showing interaction between transition metals and various concentrations of $CO_3^{2-}$. (B) The PAGE gel images showing the unloaded DNA at various metals concentrations for biomineralization, and (C) the quantification of DNA loading from B. (D) The loading efficiency of BSA at various metals concentrations for biomineralization. The biomineralization of the transition metals for various concentrations of (E) DZ and (F) GOx loading.

In this regard, inorganic nanoplatforms formed by biomineralization may offer an alternative choice, as the basic process of biomineralization is the interaction between inorganic ions (mainly metals) with biomacromolecules to form hard biomaterials [10]. Compared with organic carriers, biomineralization-based nanoparticles are advantageous for simple preparation, cost effectiveness, good physiological stability, excellent biocompatibility, and degradability [11]. Metal ions can interact with macromolecules *via* different binding force [12], such as electrostatic attraction, coordination, and hydrogen bond (*via* metal hydration), thus enabling better encapsulation efficiency and stability. For example, calcium minerals, including calcium carbonate and calcium phosphate, are the most extensively studied biomineralized carriers to deliver a broad range of drugs including nucleic acids and proteins [13,14]. Of note, transition metals are the better candidates than calcium for macromolecules binding because of their stronger coordination affinity with macromolecules [12]. However, the attempt of using transition metal as biomineralized carrier to load macromolecular drugs has been rarely explored.

Herein, we report the rational screen of biocompatible transition metal ions to biomineralize with carbonate for macromolecular drugs loading, in which $Cu^{2+}$ turns out to be the best choice with extra high loading capacity, stability, and pH-responsive drug release profile. As a proof-of-concept, copper carbonate nanoparticles were prepared to co-load glucose oxidase (GOx) and a HIF-$\alpha$ DNAzyme (DZ). Such nanomedicine could achieve multimodal tumor therapy *via* GOx-based starvation therapy, copper-based chemodynamic therapy (CDT), as well as HIF-$\alpha$ silencing for antitumor sensitization.

Various types of metal ions have been known to interact with carbonate for biomineralization [15]. Considering potential biomedical applications, several biological related and low toxic metal ions, including $Cu^{2+}$, $Fe^{2+}$, $Mn^{2+}$ and $Zn^{2+}$, were tested in this work. To conveniently evaluate their mineralization, metal ions were incubated with $CO_3^{2-}$ solutions (Fig. S1 in Supporting information), and the resulting precipitants were weighted (Fig. 1A). With fixing metal ion concentration at 100 mmol/L, the weight of precipitates gradually increased at higher carbonate anion concentrations for all types of metals. Note that, the precipitations were all formed in 1 min upon reaction, indicating their rapid mineralization. Among them, $Fe^{2+}$ produced the most abundant precipitants, and its color changed rapidly from brownish yellow to blackish green, likely due to the oxidation of the unstable $Fe^{2+}$ to $Fe^{3+}$ in test tube. As the main purpose, we screened all the biomineralized precipitation for macromolecules loading, in which a 20-nt random DNA and bovine serum albumin (BSA) was employed for proof-of-concept demonstration. With fixed BSA (0.2 mg/mL)/DNA (1 μmol/L) and $CO_3^{2-}$ (1 mmol/L) concentrations, various metal ions were titrated. The DNA was labeled with a FAM fluorophore, and the encapsulation of DNA into the biomineralized precipitation was calculated by quantifying the unloaded DNA in solution using PAGE gel electrophoresis (Fig. 1B). The loading efficiency of various metal ions was then analyzed (Fig. 1C), in which all of them could completely load the DNA at metal concentration at 0.8 mmol/L or higher, ascribing to strong and multiple binding sites between the transition metal ions and DNA. It should be also noted that $Mn^{2+}$ and $Cu^{2+}$ seemed to have better efficiency at low metal concentrations. Similarly, the unloaded BSA was measured by Bradford assay, and the result was quantified (Fig. 1D). In this case, $Cu^{2+}$ showed much better efficiency than other metals to load the protein. Therefore, biomineralization between transition metal ions and $CO_3^{2-}$ might be a promising method to load macromolecules of both nucleic acids and proteins.

To test the real applications, we further explored such strategy to load therapeutic macromolecules, in which a DNAzyme (DZ) and glucose oxidase (GOx) were employed as model therapeutic nucleic acid and protein, respectively. DNAzyme is a type of DNA-based catalyst, which could catalyze a wide range of chemical reactions [16]. Here we used an RNA-cleavage DNAzyme that can cleave the mRNA of interest for gene silencing application, and the HIF-1$\alpha$ mRNA was designed as the target since HIF-1$\alpha$ plays critical roles for tumor development, progress and metastasis [17]. GOx, on the other hand, was initially used to treat upper respiratory tract infections (NCT01883427), while recent studies have found its potential for tumor starvation therapy *via* catalytic glucose consumption [18]. Three concentrations of both DZ and GOx were tested (Figs. 1E and F), and it was found that $Cu^{2+}$ had the best loading capacity for both of them. Moreover, such biomineralization could realize DZ and GOx co-loading, and again, the $Cu^{2+}$ was the most efficient one (Fig. S2 in Supporting information). Moreover, we fur-

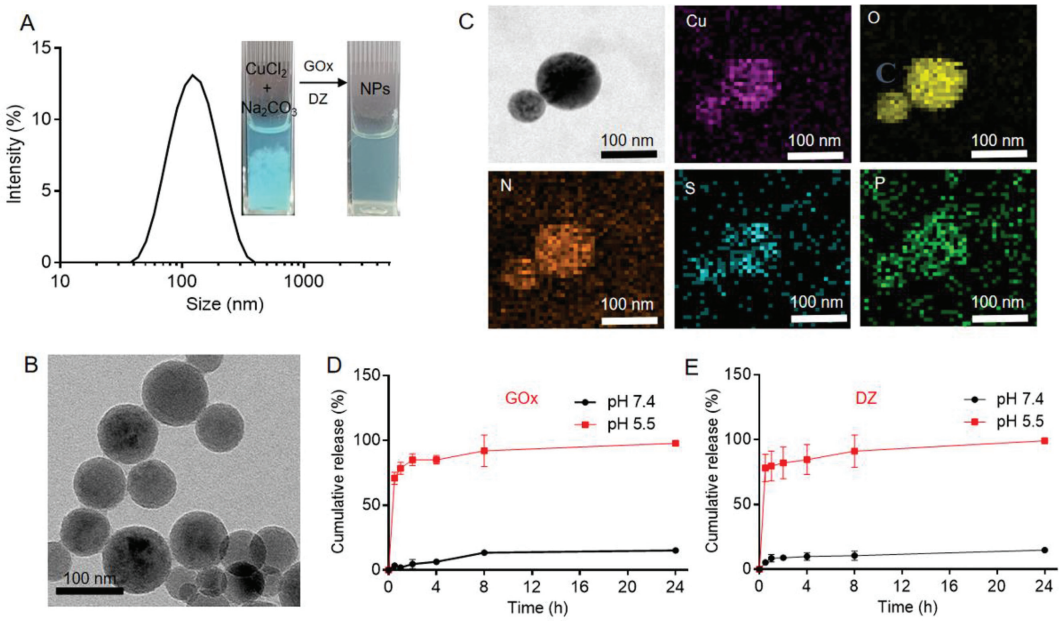


**Fig. 2.** (A) The dynamic size of GOx/DZ@Cu NPs. Inset: The appearance of the solutions before and after GOx/DZ loading to show the stabilization effect of the macromolecules. (B) TEM and (C) elemental mapping images of the nanoparticles. The pH-responsive release of (D) GOx and (E) DZ.

ther tested the extensively studied $Ca^{2+}$ for side-by-side comparison. $Cu^{2+}$ was much more efficient to biomineralize with $CO_3^{2-}$ based on the precipitant formation. Importantly, $Cu^{2+}$ showed significantly better activity to load both GOx and DZ, owing to more precipitant formation and stronger binding affinity (Fig. S3 in Supporting information).

The above experiments have indicated that the copper carbonate was the best candidate for macromolecules loading. We next explored such carrier for biomedical applications by preparing copper carbonate nanoparticles. The nanoparticles were prepared by just mixing $CuCl_2$ with GOx and DZ, followed by add $Na_2CO_3$ under ultrasonic condition. After 30 min incubation, the GOx/DZ@Cu NPs were formed showing typical Tyndall phenomenon (Fig. S4 in Supporting information). The nanoparticles had hydrodynamic size and $\zeta$ potential of ~130 nm and −12 mV, respectively (Fig. 2A and Fig. S5 in Supporting information). Interestingly, without DZ/GOx loading, such biomineralized material aggregated rapidly, suggesting a stabilization effect of the macromolecules *via* their strong interaction with the nanoparticles. From TEM, the nanoparticles showed spherical morphology with multi-dispersed size ranging from 100 nm to 200 nm (Fig. 2B). The elemental mapping was further investigated, in which the S and P elements were observed all around and outside the nanoparticles (Fig. 2C), assigning to the GOx and DZ loading. The encapsulation efficiency of GOx and DZ were further measured to be 69% and 77%, respectively, giving drug loading capacity to be 57% (for GOx) and 4% (for DZ). Therefore, overall loading capacity reached up to 61%, which was significantly higher than most organic materials, highlighting the advantage of such system for biomolecules loading.

Having confirmed the structure, we then explored the properties of the nanoparticles. First, the drug release profile was studied, in which the concentration of GOx and DZ were measured by gel electrophoresis and Bradford assay as described above. Notably, both GOx and DZ showed quite similar release profiles, in which the drugs were stably loaded under physiological mimic condition of pH 7.4, while a burst release within 1 h was observed at acidic pH of 5.5 (Figs. 2D and E). Such pH-responsive property is highly appreciable for drug delivery, since it can prevent pre-mature drug release during *in vivo* circulation, while rapidly release drugs upon reaching the target cells. Actually, the carbonate-based metal nanoparticles share the similar pH-responsive property, in which the calcium carbonate is the most extensively studied one [13]. The common mechanism is the dissolution of $CO_3^{2-}$ at acidic condition, accompanied by the release of the drugs. The nanoparticle dissolution was further probed by centrifugation, in which almost no precipitation was observed after acidic pre-treatment (Fig. S6 in Supporting information).

Different from small molecular drugs, one key consideration of macromolecules delivery is their retained biofunctions after being delivered to the target site. GOx could catalyze the oxidization of glucose into gluconic acid and hydrogen peroxide ($H_2O_2$) with consumption of molecular oxygen. Therefore, the activity of GOx can be easily monitored by measuring $O_2$ and pH decrease. At pH 7.4, the GOx/DZ@Cu NPs did not show any catalytic activity, due to the passivation of GOx upon loading into nanoparticles (Figs. S7 and S8 in Supporting information). Notably, such deactivation is meaningful to decrease the side-effect of GOx during circulation, *i.e.*, the catalytic consumption of glucose to cause glycopenia [19]. With acidic buffer pre-treatment, an obvious catalytic activity was observed for GOx/DZ@Cu NPs, attributable to the collapse of the nanoparticles to release GOx. Notably, its activity could recover to the level compatible to free GOx (Fig. S9 in Supporting information), indicating that the biomineralized encapsulation has little effect on biofunction of the enzyme. Meanwhile, the catalytic activity of the DZ to cleavage target mRNA was tested. Free DZ could effectively cleave the substrate in presence of the intracellular abundant $Mg^{2+}$ to produce the cleaved band on gel image (Fig. S10 in Supporting information). For GOx/DZ@Cu NPs, the cleavage was only observed at pH 5.5 buffer, consistent with the above results, which was also ascribed to the pH-dependent release of DZ.

Compared to the widely studied calcium carbonate, one extra merit of copper carbonate nanoparticles is the pH-responsive release of copper ion to induce tumor chemodynamic therapy (CDT) *via* Fenton-like reaction. To demonstrate this, the GOx/DZ@Cu NPs was pre-treated with acidic buffer to release $Cu^{2+}$, followed by adding $H_2O_2$ and GSH. GSH could reduce $Cu^{2+}$ into $Cu^{+}$, which then decomposes $H_2O_2$ into toxic $^{\bullet}OH$. The $^{\bullet}OH$ generation was probed by methylene blue (MB), which could be rapidly degraded

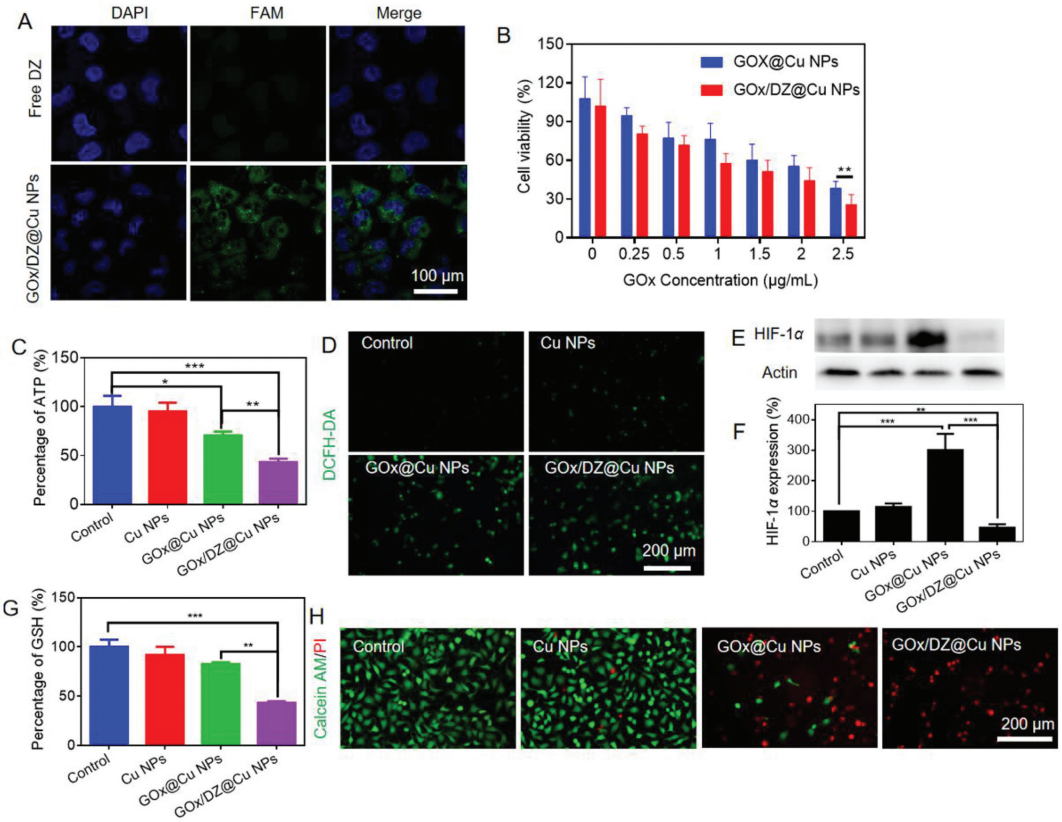


**Fig. 3.** (A) Fluorescent images showing the uptake of free DZ and GOx/DZ@Cu NPs. (B) The cell cytotoxicity of GOx@Cu and GOx/DZ@Cu NPs. (C) The relative intracellular ATP level after various treatments. (D) The DCFH-DA fluorescence to probe the intracellular ROS generation after various treatments. (E) HIF-1$\alpha$ protein expression after various treatments, and (F) the protein level quantification. (G) The relative intracellular GSH level after various treatments. (H) Fluorescent image of live/dead cell staining to show the anti-tumor activity of various formulations.

by $^{\bullet}OH$ accompanied by the decrease of UV–vis absorbance at 664 nm. As expected, the released $Cu^{2+}$ from GOx/DZ@Cu NPs after acidic pre-treatment could induce a strong CDT effect, while such Fenton effect was much weaker under physiological condition (pH 7.4) owing to pH responsive release of $Cu^{2+}$ (Fig. S11 in Supporting information). Of note, GOx/DZ@Cu NPs with GOx loading could catalyze the $H_2O_2$ generation during glucose consumption, which further boosts the CDT efficacy. To confirm this, free glucose was added instead of $H_2O_2$, and as expected, a concentration dependent CDT effect was observed (Fig. S12 in Supporting information). Therefore, the co-loaded GOx could not only exert tumor starvation therapy *via* glucose consumption, but also promote the CDT through catalytic generation of $H_2O_2$, achieving a synergistic effect.

Next, the intracellular performances of the nanoparticles were explored by using M231 breast cancer as example. To explore the cell transport, the loading DZ was labeled with FAM fluorophore, and the cell nuclei were stained blue by Hoechst 33342. As a common limitation, the macromolecules usually have low cell penetration efficiency, and thus transfection reagents are required. The negatively charged DNA is repelled by cell membrane, resulting in extremely weak fluorescence inside cells for free DZ (Fig. 3A). For GOx/DZ@Cu NPs, by contrast, the cells emitted bright fluorescence, suggesting nanoparticles-mediated DZ delivery. Therefore, the Cu NPs could serve as an effective carrier for intracellular delivery of macromolecules.

The anti-tumor activity was then evaluated by MTT assay [20]. In absence of the payloads, the Cu NPs did not show any cytotoxicity at concentration up to 25 μmol/L (Fig. S13 in Supporting information), which can be explained by the poor CDT effect with limited level of $H_2O_2$ inside cells. Therefore, Cu NPs alone was a biocompatible material. With GOx loading (the nanoparticles termed GOx@Cu NPs), a concentration-dependent decrease of cell viability was seen (Fig. 3B), attributable to catalytic starvation therapy. To confirm this, the intracellular ATP level was measured (Fig. 3C). GOx@Cu NPs could significantly reduce the ATP level, verifying the blockage of energy supply. Moreover, the GOx-catalyzed generation of $H_2O_2$ would also contribute to the enhanced antitumor effect by promoting CDT. To probe this, ROS generation, the biomarker of CDT, was visualized by using 2′,7′-dichlorofluorescin diacetate (DCFH-DA) indicator with green fluorescence. Compared to the control, Cu NPs barely showed any fluorescence, confirming its weak CDT effect (Fig. 3D). However, a strong fluorescence was noticed for the cells with GOx@Cu NPs treatment, indicating the sensitization of GOx on CDT.

Interestingly, the additional DZ loading could further promote anti-tumor effect (Fig. 3B), resulting in 27.8% lower $IC_{50}$ value of GOx/DZ@Cu NPs than that of GOx@Cu NPs. The enhanced effect can be ascribed to DZ-mediated HIF-1$\alpha$ suppression, which has been confirmed by Western blot analysis of this protein (Figs. 3E and F), and several mechanisms can explain such results. First, the GOx-mediated starvation therapy exacerbates the tumor hypoxia *via* oxygen consumption, which in turn stimulates the upregulation of HIF-1$\alpha$ to adapt tumor hypoxia with better survival. Our result also confirmed this effect with significantly upregulation of HIF-1$\alpha$ with GOx@Cu NPs therapy. GOx/DZ@Cu NPs treatment, by contrast, significantly suppressed the expression of HIF-1$\alpha$, confirming the intracellular activation of the DZ. Meanwhile, the regulation of HIF-1$\alpha$ could also reverse the cell oxidative protection system, as evidenced by the decrease of GSH level, the major anti-oxidant system inside cells, after GOx/DZ@Cu NPs treatment (Fig. 3G) [21]. Therefore, DZ-induced HIF-1$\alpha$ inhibition could block all these negative effects to sensitize both starvation therapy and CDT.

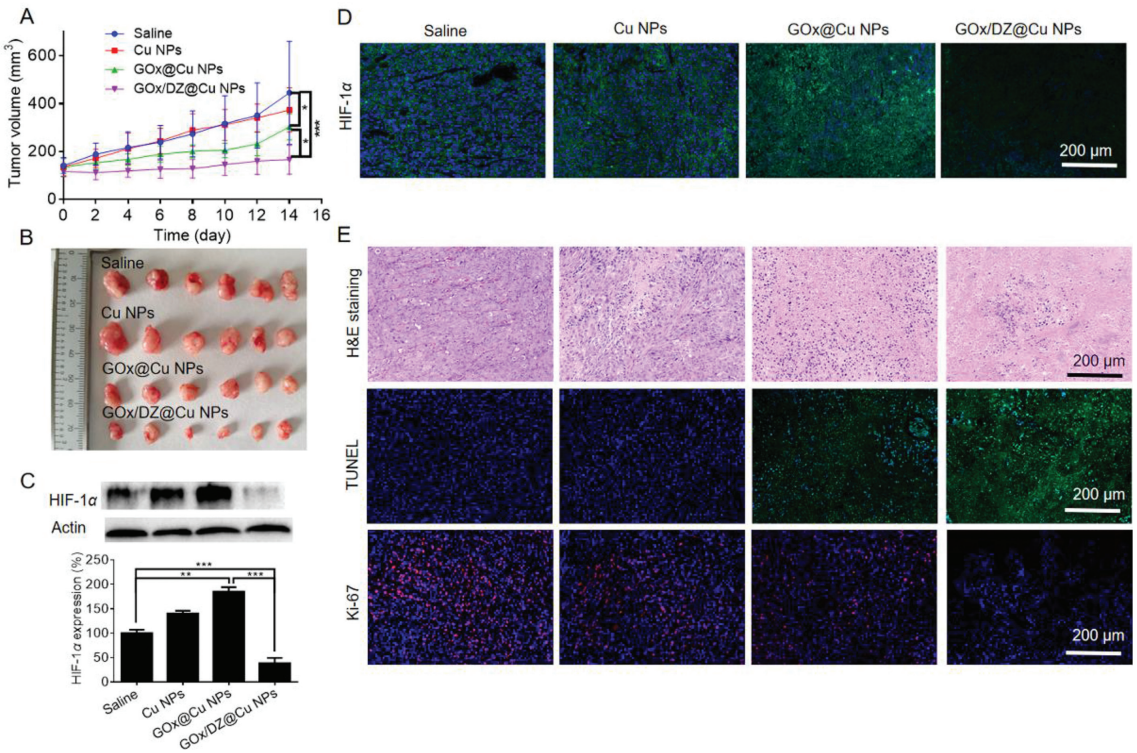


**Fig. 4.** (A) Tumor growth kinetics during various treatments. (B) The appearance of the tumors after various treatments. (C) The Western blot and (D) immunofluorescence assay to analyze the HIF-1$\alpha$ expression after various treatments. (E) H&E staining, TUNEL and Ki-67 fluorescent staining of the tumor tissues after various treatments.

To further confirm the antitumor activity, we next performed the live/dead cell staining assay, in which the live cells and dead cells were stained with Calcein-AM (green fluorescence) and PI (red fluorescence), respectively. Bright green fluorescence was seen inside cells after Cu NPs treatment, confirming the minimal cytotoxicity of the nanoparticles. For GOx/DZ@Cu and GOx@Cu groups, on the contrary, the red fluorescence became intensified with a large number of cells being dead. Among various treatment, GOx/DZ@Cu produced the highest intensity of red fluorescence, consistent with the above results (Fig. 3H).

Finally, the *in vivo* behavior of GOx/DZ@Cu NPs was explored by using M231 tumor-bearing mice. All experimental procedures were approved by the Ethics Committee for Research in Animal Subjects at Xiangya School of Pharmaceutical Sciences of Central South University. Owing to its high hemocompatibility (Fig. S14 in Supporting information), the nanoparticle was administrated *via* tail intravenous injection. To study the biodistribution, the DZ was labeled with a Cy5.5 NIR fluorophore for *in vivo* imaging using the IVIS Lumia XRMS series III system. Free DZ or GOx/DZ@Cu NPs were injected when the tumor volume reached about 100 $mm^3$. At 1 h post injection, free DZ showed high fluorescence throughout the body (Fig. S15A in Supporting information), indicating nonspecific distribution, while the fluorescence was strongly weakened at 24 h, due to the rapid degradation and clearance of the nucleic acids. Because of the fluorescence quenching effect, GOx/DZ@Cu NPs initially emitted weak fluorescence at 1 h, but the fluorescence was recovered at 24 h, suggesting a long circulation effect of the nanoparticles. Specifically, we observed a notable signal at tumor site for GOx/DZ@Cu NPs. To verify this, the tumor tissue and major organs were extracted at 24 h post-injection for ex vivo fluorescence imaging and quantification (Fig. S15B in Supporting information). Obviously, GOx/DZ@Cu NPs exhibited higher intensity at tumor site than free DZ, confirming targetability of the nanoparticles to accumulate into tumor *via* EPR effect. Meanwhile, we also noticed considerable accumulation of NPs in liver and kidneys, which were the main organs to sequester and eliminate NPs from body.

To explore the anti-tumor activity, the tumor-bearing mice were randomly divided into four groups ($n = 6$), each receiving one of the following treatments: saline (control), Cu NPs, GOx@Cu NPs and GOx/DZ@Cu NPs (with an equivalent GOx dosage of 2 mg/kg), respectively. The anti-tumor effect was dynamically monitored every other day by measuring the tumor volume. Compared to the control, only marginal tumor growth inhibition was observed for Cu NPs (Fig. 4A). With GOx encapsulation, the anti-tumor effect of GOx@Cu NPs was significantly enhanced. Notably, the best efficacy was observed for GOx/DZ@Cu NPs, achieving 83% tumor growth suppression efficiency. For convenient observation, the tumor was collected and weighted after treatments (Fig. 4B and Fig. S16 in Supporting information), and the overall therapeutic efficacy was in order of GOx/DZ@Cu NPs > GOx@Cu NPs > Cu NPs. Therefore, the combination of DZ could sensitize the efficacy of both CDT and starvation therapy *via* its HIF-1$\alpha$ regulation effect. To confirm the *in vivo* activation of DZ, the expression of HIF-1$\alpha$ was investigated by both western blot and immunofluorescence assay (Figs. 4C and D). While Cu NPs has little marginal effect, GOx@Cu NPs could significantly promote the expression of HIF-1$\alpha$ owing to the catalytic $O_2$ consumption to exacerbate tumor hypoxia. With DZ co-loading, GOx/DZ@Cu NPs could reverse the adverse effect of GOx to effectively downregulate HIF-1$\alpha$, which in turn contributed to the enhanced tumor therapy. The anti-tumor activity was further evaluated by pathologically analyzing the tumor tissue. After GOx/DZ@Cu NPs therapy, the tumor tissue showed the highest level of cell necrosis, apoptosis, as well as the most significant inhibition of proliferation based on H&E, TUNEL, and Ki67 staining, respectively (Fig. 4E). Collectively, all these results demonstrated the superiority of GOx/DZ@Cu for tumor therapy.

The biocompatibility of the nanosystem were evaluated systematically. The body weight of all mice did not change obviously during treatment (Fig. S17 in Supporting information), indicating

no acute toxicity. After treatments, several blood biochemical indexes, including liver enzymes alanine transaminase (ALT), aspartate aminotransferase (AST), blood urea nitrogen (BUN), and creatinine (Cre), were within the normal range (Fig. S18A in Supporting information), demonstrating the lack of hepatotoxicity and nephrotoxicity. Moreover, the major organs were further examined by H&E staining (Fig. S18B in Supporting information), and no pathological change was observed, demonstrating the biosafety of the nanoparticles for *in vivo* applications.

In summary, we report a highly robust Cu NPs as a biomineralized carrier of macromolecules with extremely high loading capacity and pH-responsive drug release profile. $Cu^{2+}$ was rationally screened from various transition metals based on their properties to biomineralize with $CO_3^{2-}$ for both nucleic acids and protein loading. Cu NPs was prepared through a simple process to effectively load GOx and DZ as co-delivery system, and facilitate their delivery for tumor accumulation and cell membrane penetration. From therapeutic aspect, GOx/DZ@Cu acted as an all-in-one nanoplatform to exert combinatorial starvation therapy/gene therapy/CDT *via* co-release of GOx, DZ and $Cu^{2+}$, achieving excellent anti-tumor effect. Collectively, such biocompatible nanoplatform with facile and cost-effective preparation, robust drug loading, and multiple functionalities shows great promise as a general carrier for micromolecular drugs to promote their clinical translation.

## Declaration of competing interest

The authors declare that they have no known competing financial interests or personal relationships that could have appeared to influence the work reported in this paper.

## Acknowledgments

This work was supported by National Natural Science Foundation of China (Nos. U1903125, 82073799), Natural Science Foundation of Hunan Province in China (No. 2021JJ20084), the Science and Technology Innovation Program of Hunan Province (No. 2021RC3020), Training Program for Excellent Young Innovators of Changsha (No. kq2206057), and the Hunan Provincial Education Commission Foundation (Nos. 19B068, 20A056).

## Supplementary materials

Supplementary material associated with this article can be found, in the online version, at doi:10.1016/j.cclet.2023.108192.

## References

[1] M. Rütter, N. Milošević, A. David, J. Control. Release 330 (2021) 1191–1207.
[2] P. Tyagi, J.L. Santos, Drug Discov. Today 23 (2018) 1053–1061.
[3] L. Guo, S. Zhong, P. Liu, M. Guo, J. Ding, W. Zhou, Small 18 (2022) e2202604.
[4] W. Sun, Y. Xu, Y. Yao, et al., J. Nanobiotechnol. 20 (2022) 88.
[5] Q. Guo, C. Jiang, Acta Pharm. Sin. B 10 (2020) 979–986.
[6] Y. Song, Y. Huang, F. Zhou, J. Ding, W. Zhou, Chin. Chem. Lett. 33 (2022) 597–612.
[7] R. Liu, C. Luo, Z. Pang, et al., Chin. Chem. Lett. 34 (2023) 107518.
[8] J. Deng, R. Wang, S. Huang, J. Ding, W. Zhou, Chin. Chem. Lett. 34 (2023) 107588.
[9] B. Hu, L. Zhong, Y. Weng, et al., Signal. Transduct. Target. Ther. 5 (2020) 101.
[10] W. Wang, X. Liu, X. Zheng, H.J. Jin, X. Li, Adv. Healthc. Mater. 9 (2020) e2001117.
[11] S. Yao, B. Jin, Z. Liu, et al., Adv. Mater. 29 (2017) 1605903.
[12] N.H.E. Khare, M.J. Buehler, Nat. Rev. Mater. 6 (2021) 421–436.
[13] C. Xu, Y. Yan, J. Tan, et al., Adv. Funct. Mater. 29 (2019) 1808146.
[14] D.S. Maleki, S. Sharifi, E. Ahmadian, et al., Expert. Opin. Drug Deliv. 16 (2019) 331–345.
[15] S.E. Wolf, L. Müller, R. Barrea, et al., Nanoscale 3 (2011) 1158–1165.
[16] W. Zhou, R. Saran, J. Liu, Chem. Rev. 117 (2017) 8272–8325.
[17] X. Jing, F. Yang, C. Shao, et al., Mol. Cancer 18 (2019) 157.
[18] L.H. Fu, C. Qi, J. Lin, P. Huang, Chem. Soc. Rev. 47 (2018) 6454–6472.
[19] Y. Zeng, H. Zhou, J. Ding, W. Zhou, Theranostics 11 (2021) 8270–8282.
[20] J.S. Cao, C. Chen, Y.H. Wang, et al., Oncol. Lett. 12 (2016) 2033–2037.
[21] Z.H. Zhao, J. Yan, K. Ling, et al., Adv. Funct. Mater. 31 (2021) 2106471.